[4] J. Xu, Z. R. Liu, R. Liu, and Q. F. Yang, "Information transmission in human cerebral cortex," *Physica D*, vol. 106, pp. 363–374, Aug. 1997.
[5] X. S. Zhang, R. J. Roy, and E. W. Jensen, "EEG complexity as a measure of depth of anesthesia for patients," *IEEE Trans. Biomed. Eng.*, vol. 48, no. 12, pp. 1424–1433, Dec. 2001.
[6] D. Abásolo, R. Hornero, C. Gómez, M. García, and M. López, "Analysis of EEG background activity in Alzheimer's disease patients with Lempel-Ziv complexity and central tendency measure," *Med. Eng. Phys.*, vol. 28, no. 4, pp. 315–322, May 2006.
[7] C. Gómez, R. Hornero, D. Abásolo, A. Fernández, and M. López, "Complexity analysis of the magnetoencephalogram background activity in Alzheimer's disease patients," *Med. Eng. Phys.*, vol. 28, no. 9, pp. 851–859, Nov. 2006.
[8] V. D. Gusev, L. A. Nemytikova, and N. A. Chuzhanova, "On the complexity measures of genetic sequences," *Bioinformatics*, vol. 15, no. 12, pp. 994–999, Dec. 1999.
[9] R. Nagarajan, "Quantifying physiological data with Lempel-Ziv complexity—Certain issues," *IEEE Trans. Biomed. Eng.*, vol. 49, no. 11, pp. 1371–1373, Nov. 2002.
[10] M. Aboy, R. Hornero, D. Abásolo, and D. Álvarez, "Interpretation of the Lempel—Ziv complexity measure in the context of biomedical signal analysis," *IEEE Trans. Biomed. Eng.*, vol. 53, no. 11, pp. 2282–2288, Nov. 2006.
[11] F. Michard, S. Boussat, D. Chemla, N. Anguel, A. Mercat, Y. Lecarpentier, C. Richard, M. R. Pinsky, and J. L. Teboul, "Relation between respiratory changes in arterial pulse pressure and fluid responsiveness in septic patients with acute circulatory failure," *Amer. J. Respir. Critical Care Med.*, vol. 162, no. 1, pp. 134–138, July 2000.
[12] C. K. Hofer, S. M. Müller, L. Furrer, R. Klaghofer, M. Genoni, and A. Zollinger, "Stroke volume and pulse pressure variation for prediction of fluid responsiveness in patients undergoing off-pump coronary artery bypass grafting," *Chest*, vol. 128, no. 2, pp. 848–854, Aug. 2005.
[13] A. Kramer, D. Zygun, H. Hawes, P. Easton, and A. Ferland, "Pulse pressure variation predicts fluid responsiveness following coronary artery bypass surgery," *Chest*, vol. 126, no. 5, pp. 1563–1568, Nov. 2004.
[14] F. Michard and J. L. Teboul, "Predicting fluid responsiveness in ICU patients: A critical analysis of the evidence," *Chest*, vol. 121, no. 6, pp. 2000–2008, June 2002.
[15] J. Bajorat, R. Hofmockel, D. A. Vagts, M. Janda, B. Pohl, C. Beck, and G. Noeldge-Schomburg, "Comparison of invasive and less-invasive techniques of cardiac output measurement under different haemodynamic conditions in a pig model," *Eur. J. Anaesthesiol.*, vol. 23, no. 1, pp. 23–30, Jan. 2006.
[16] M. Aboy, J. McNames, T. Thong, C. R. Phillips, M. S. Ellenby, and B. Goldstein, "A novel algorithm to estimate the pulse pressure variation index deltaPP," *IEEE Trans. Biomed. Eng.*, vol. 51, no. 12, pp. 2198–2203, Dec. 2004.

DCT-Based Complexity Regularization for EM Tomographic Reconstruction

Max Mignotte*, Jean Meunier, and Jean-Paul Soucy

***Abstract*—This paper introduces a simple algorithm for tomographic reconstruction based on the use of a complexity regularization term. The regularization is formulated in the discrete cosine transform (DCT) domain by promoting a low-noise reconstruction having a high sparsity in the frequency domain. The resulting algorithm simply alternates between a maximum-likelihood (ML) expectation-maximization (EM) update and a decreasing sparsity constraint in the DCT domain. Applications to SPECT reconstruction and comparisons with a classical estimator using the best available regularization terms are given in order to illustrate the potential of our reconstruction technique.**

***Index Terms*—Discrete cosine transform (DCT), expectation-maximization (EM), reconstruction, SPECT tomography.**

I. Introduction

A major challenge for Bayesian image reconstruction algorithms is the design of efficient image prior models summarizing the intrinsic properties of the object being evaluated. This allows to restrict the types of reconstructions (*a priori*) defined as acceptable solutions.

Except for wavelet-based regularization methods, little attention has been given to the use of complexity-based regularization in Bayesian tomographic reconstruction. Wavelet-based methods exploit the sparsity of the wavelet coefficients by using either prefiltering of the acquired raw-data [1], postfiltering of the reconstructed images [2], [3], or a regularization strategy during the optimization process, using a maximum *a posteriori* (MAP) formulation [4]–[6].

In such a framework, the simple discrete cosine transform (DCT) could also be used to constrain the problem of reconstruction from projections. As opposed to the widely used wavelet transform, this transform can be used locally, by using a strategy of local filtering on (overlapping) individual blocks. Therefore, this local filtering approach also allows to take into account, indirectly, the nonstationarity property of the object being reconstructed.

What we propose in this paper is a simple and efficient, DCT-based reconstruction method which alternates between a maximum-likelihood (ML) EM update and DCT-based filtering, using an easily implemented decreasing thresholding rule. The potential of this reconstruction technique will be illustrated through a series of examples reconstructed both with this approach and a more classic estimator using the best available regularization terms.

II. Bayesian Tomographic Reconstruction

Reconstructing an emission tomography study can be considered in a statistical framework where we consider a pair of random fields (Y, X),

Manuscript received February 28, 2007; revised May 10, 2007. This work was supported by research grant from the Natural Sciences and Engineering Council of Canada (NSERC). *Asterisk indicates corresponding author.*

*M. Mignotte is with the Département d'Informatique et de Recherche Opérationnelle (DIRO), Université de Montréal, C.P. 6128, Succ. Centre-ville, Montréal H3C 3J7, QC, Canada (e-mail: mignotte@iro.umontreal.ca).

Meunier is with the Département d'Informatique et de Recherche Opérationnelle (DIRO), Université de Montréal, Montréal H3C 3J7, QC, Canada .

J.-P. Soucy is with the Research Center of the University of Montréal Medical Center, Montréal H2L 4M1, QC, Canada (e-mail: jean-paul.soucy.chum@ssss.gouv.qc.ca).

Color versions of one or more of the figures in this paper are available online at http://ieeexplore.ieee.org.

Digital Object Identifier 10.1109/TBME.2007.912635

where Y is an M-dimensional vector of Poisson-distributed photon counts and X is an N-dimensional random vector of emission rates. A particular realization of these random vectors are, respectively, y_i, designating the number of counts received at detector bin i, and x_j, representing the mean emission rate from voxel j. Let $\mathcal{H}$ model a discrete Radon transform, i.e., the $M \times N$ system matrix $\mathcal{H}$ with elements $\mathcal{H}_{ij}$ proportional to the probability of receiving a count in detector element i from voxel j. According to the standard emission tomographic model in which the sinograms y_i are independently Poisson distributed, the log-likelihood function can be written as [7]

$$\log P_{Y|X}(y|x) \propto -\sum_{i=1}^{M}\left\{y_i \log\left[\sum_{j=1}^{N}\mathcal{H}_{ij}\, x_j\right] - \sum_{j=1}^{N}\mathcal{H}_{ij}x_j\right\} = -\Phi_L(y;x). \quad (1)$$

Combining this log-likelihood distribution with an *a priori* distribution of the form $P_X(x) \propto \exp\{-\gamma\Omega(x)\}$, for the set of feasible reconstructions, leads to the following energy minimization problem, the solution of which is a tomographic reconstruction in the MAP sense, $\hat{x}_{\mathrm{MAP}} = \arg\min_x\{\Phi_L(y;x) + \gamma\,\Omega(x)\} = \arg\min_x\{E(x)\}$. In order to minimize such an energy function, we use a classical iterative EM one step late (EM-OSL) algorithm [7] (or its variation based on the use of an ordered subset processing, [8] which speeds up convergence). The resulting EM-OSL update equation is

$$\hat{x}_j^{[n+1]} = \hat{x}_j^{[n]} \frac{\sum_{i=1}^{M}\mathcal{H}_{ij}\,\frac{y_i}{\sum_{j=1}^{N}\mathcal{H}_{ij}\,\hat{x}_j^{[n]}}}{\sum_{i=1}^{M}\mathcal{H}_{ij} + \gamma\,\frac{\partial}{\partial x_j}\,\Omega(x_j = \hat{x}_j^{[n]})} \quad (2)$$

where $\Omega(x)$ is the regularization term used (see Section V for a list of the regularization terms tested in this paper). The quality of the reconstructed image will closely depend on this term and its ability to model the intrinsic properties of the object being evaluated. Another regularization strategy used in our application consists in sequentially and repeatedly applying the unregularized version of this algorithm (i.e., $\Omega(x) = 0$, which is the well-known ML-EM algorithm [9], [10]), and a denoising step based on complexity. Silverman *et al.* in [11] proposed a similar strategy in which the so-called EMS algorithm consisted in alternating a ML-EM-like iteration with a smoothing step (for which a variety of median and averaging filters were proposed and studied) for tomographic reconstruction.

III. Proposed Regularization Strategy

In order to regularize the noisy solution obtained after each iteration of the ML-EM algorithm, we *a priori* restrict the admissible solutions to a class of images with a sparse DCT transform representation. Using this (regularized) image model, the proposed denoising approach then consists in applying a frequential filtering based on the DCT transform of each 8 × 8 subimage extracted from the current reconstructed version of the image. For the filtering operation in the DCT domain, we have chosen the easily-implemented hard thresholding rule [12] also classically used in wavelet-based denoising approaches, (cf. Algorithm 1) where γ_{T} is a threshold level and w is one of the coefficients obtained by the DCT transform of the block (of size 8 × 8 pixels) extracted from the current image estimate. In order to reduce blocky artifacts across block boundaries, we adopted a standard approach where this transform is made translation-invariant, by using the DCT of all (circularly) translated version of the image (herein assumed to be toroidal) [13], [14] (this implies computing a set of eight horizontal shifts and eight vertical shifts ($= 64$) transformed images) which will then be averaged in the final step of this denoising procedure.

DCT-Based Denoising Step

$x^{[n]}$ Input image to be denoised at iteration n
$\hat{x}^{[n]}$ Denoised estimated image at iteration n
γ_{T} Threshold

for *All (8 horiz. and 8 vert.) shifts of* $x^{[n]}$ **do**
  for *All* $[8 \times 8]$ *blocks extracted from* $x^{[n]}$ **do**
    1. DCT Transform
    2. Threshold the obtained DCT coefficients w with the hard thresholding rule

$$w_T^{\text{hard}} = \begin{cases} 0 & \text{if } |w| \leq \gamma_{\mathrm{T}} \\ w & \text{otherwise} \end{cases}$$

    3. Inverse DCT of these thresholded coef.
  ▷ Unshift the filtered image and store it

$\hat{x}^{[n]} \leftarrow$ Averaging of these 64 denoised images

Algorithm 1. DCT-based denoising step.

In order to improve the regularization, and to make it somewhat adaptive, we also propose to compare the reconstruction results with a variant consisting in decreasing, during the iterative EM procedure, the threshold value to a minimal value, following a procedure resembling a cooling threshold schedule. To this end, we use an empirical geometrically decreasing law for the threshold $\max(\gamma \cdot (0.86)^n, \gamma/6)$ where n is the number of iterations. This regularization process gives a stronger sparsity constraint for the first steps (during which the reconstruction procedure exhibits a very noisy estimate) and a lower sparsity constraint at the end when the reconstructed estimate is already significantly denoised and deblurred.

IV. Data Sets

To test our proposed solution, we have first used a $N = 128 \times 128$ pixel (with 32 different grey level values) simulation of a brain SPECT slice with a (relatively) realistic spatial distribution of the three main anatomical tissue types (gray and white matter, cerebro-spinal fluid) [Fig. 3(a)], obtained by reconstructing projections blurred by a Gaussian smoothing filter to reproduce the effect of the uncertainty in the exact location of a detected event, and then corrupted with Poisson noise [15].

We also tested our technique on actual SPECT[1] data, acquired from a phantom consisting in a large plastic cylinder containing four vials (of two different sizes) having different concentrations of a radioactive isotope (99mTc) (see Fig. 4 for the radioactivity concentration). Knowing both the geometry of the phantom and the radioactivity concentration within each subcompartment, we have generated a cross-sectional "ground truth" (cf. Fig. 4) which will be compared, after registration, with the best reconstruction results obtained by the different reconstruction techniques tested. These best reconstruction results will be defined as the closest to ground truth reconstruction (in the SNR sense) amongst the ones obtained from different values of γ, the regularization (2), or the thresholding parameter (Algorithm 1).

[1]acquired on a triple-head camera (Picker Prism) equipped with low-energy, high-resolution parallel-holes collimators. The projections over 360° were simultaneously acquired using a 20% energy window centered on the 140 keV (126–154 keV) photopeak and a Compton window (111–125 keV) (the Compton projections are subtracted, position by position, from the photopeak projection (after scaling the Compton images to 40%), before reconstruction). Acquisition time was 40 s/projection. Each SPECT data set contains 90 projections (obtained at equally spaced angles over 360°) on 128 × 128 matrices resulting in 1.86-mm isotropic voxels in the reconstructed volume.

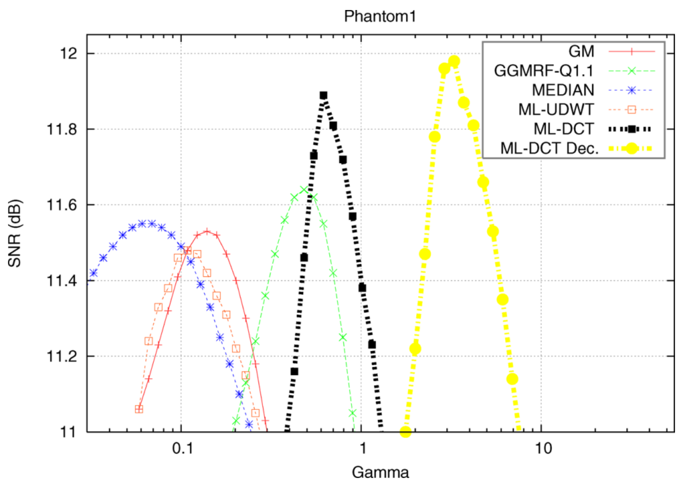

Fig. 1. Signal-to-noise (SNR) results for the synthetic phantom image presented in Fig. 4 with its degradation model as a function of the regularization parameter γ. Maximal SNR value, respectively, GM: SNR $= \mathbf{11.53}$ dB ($\gamma = \mathbf{0.14}$), GGMRF$_{q=1.1}$: SNR $= \mathbf{11.64}$ dB ($\gamma = \mathbf{0.48}$), MEDIAN : SNR $= \mathbf{11.55}$ dB ($\gamma = \mathbf{0.07}$), ML-UDW : SNR $= \mathbf{11.48}$ dB ($\gamma = \mathbf{0.11}$), ML-DCT: SNR $= \mathbf{11.89}$ dB ($\gamma = \mathbf{0.62}$), ML-DCT$_{\mathrm{Dec.Thresh.}}$: SNR $= \mathbf{11.98}$ dB ($\gamma = \mathbf{3.29}$).

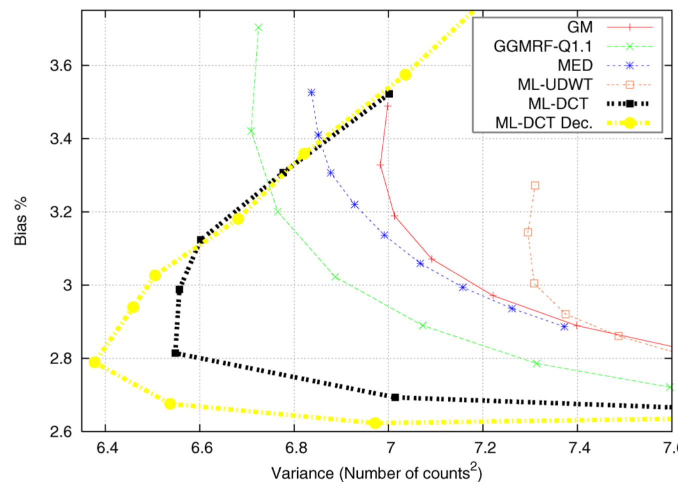

Fig. 2. Bias-variance reconstruction performance of each algorithm as a function of the regularization parameter γ.

V. Setup

Algorithm

We initialize each reconstruction method with a reconstructed image obtained with a classical filtered back projection (FBP) algorithm. As suggested in [16], we correct the zero-frequency component of the initial condition with a least-squares estimate directly from the data.

For the denoising step, in order to speed up the procedure (without degrading the reconstruction results), we use an overlap of three pixels for the sliding 8×8 window and a random shift procedure for each iteration of the algorithm (instead of considering all eight horizontal and eight vertical shifts).

The convergence criterion of the proposed restoration procedure is defined either as stability of the MAP energy $E(\hat{x})$, i.e., $[E(\hat{x}^{[n]}) - E(\hat{x}^{[n-1]})]/E(\hat{x}^{[n]}) \leq \delta$ where δ is a threshold, typically set, in our application, to 10^{-4}, or as stability of the reconstructed image.

A. Comparisons and Validation Protocol

We have compared amongst themselves the following reconstruction models [compatible with the penalized ML-EM iterative method presented in (2)]: the Gaussian Markov prior [17], the generalized Gaussian MRF prior [16], [18], the Median Prior [19] and finally, our DCT-based denoising strategy with and without the threshold cooling schedule. We also compare this strategy with a denoising step using a hard thresholding of undecimated discrete (redundant nonorthogonal and shift invariant) wavelet (UDW) [20] coefficients (with three levels of resolution) which seems to be one of the most promising wavelet decomposition technique in the context of image denoising for optical images [21]. The quantitative value we selected to compare the different algorithms is the SNR (and the resulting reconstructed image) associated with the lowest MAP energy (or the lowest penalized ML for the strategies using a denoising step).

For the first phantom, we have also done a bias/variance analysis of each tested reconstruction strategy (see Fig. 2) by adding the weighted (given by the empirical proportion) bias and variance obtained on each class of the synthetic phantom. In the obtained bias/variance graphs, the lower right hand corner of the plots corresponds to weak regularization (low bias with high variance), whereas the upper left hand corner corresponds to strong regularization (high bias with low variance).

VI. Experimental Results

1) Results on Synthetic Images: Fig. 1 summarizes the different SNRs obtained on the synthetic phantom as a function of the parameter γ for, respectively, the Gaussian Markov prior (abbrev. GM), the generalized Gaussian MRF prior with $q = 1.1$ (GGMRF$_{q=1.1}$), the median prior (MEDIAN), the ML-EM iteration using a hard thresholding of undecimated wavelet coefficients and the proposed strategy (ML-DCT) using a hard thresholding of DCT coefficients or a cooling threshold schedule (ML-DCT Dec.). In Fig. 3 we give examples of the best reconstructions (in the SNR sense) obtained with these different prior models for this synthetic phantom. Quantitative comparison between these different reconstruction strategies are also given in Fig. 2 in terms of bias-variance tradeoff. Our DCT-based methods outperform the other reconstruction technique in all cases.

2) Results on a Physical SPECT Phantom: In this experiment, assessment of the results in terms of resolution can be made either by visual comparison to the ground truth image (cf. Fig. 4) or by comparing the different SNR result obtained with the different reconstruction methods. Once again, we can see that our regularization strategy performs very competitively, exhibiting low MSE error, high SNR results, and good reconstruction of shapes.

A. Discussion

As can be seen in Fig. 3, our DCT-based complexity regularization strategy allows efficient preservation of the edges of the object being evaluated and thus good recovery of the very small structures of the phantom. This edge preserving property is achieved in the frequency domain in a manner similar to that of the EM-UDWT method, which uses a frequential nonorthogonal redundant wavelet-based denoising scheme. However, contrary to the wavelet denoising procedure, which remains a global denoising process (achieved at each iteration of the ML-EM algorithm), the proposed DCT-based denoising procedure uses a semi-global strategy (or, more exactly, a local filtering on overlapping individual block of size 8×8 pixels). This strategy is therefore robust to nonstationarities of the object to be reconstructed and also takes into account the nonstationarities of the noise process.

The improvement in term of SNR, MSE, or bias/variance reconstruction performance is especially visible where the object being evaluated

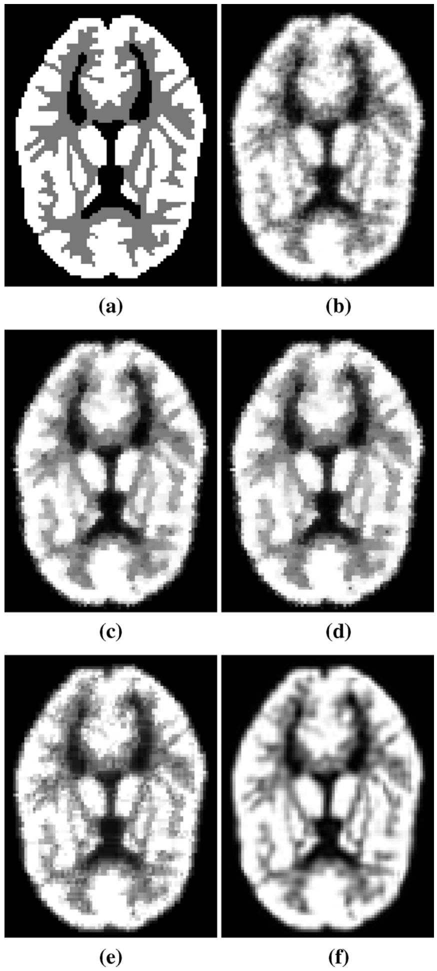

Fig. 3. Top left: (a) Original SPECT phantom 128 × 128 synthetic phantoms with a quantification of 32 different grey level values (totalizing 7 161 K total counts). (b) GM: 11.53 dB. (c) GGMRF$_{q=1.1}$: 11.64 dB. (d) MEDIAN: 11.55 dB. (e) EM-UDWT: 11.48 dB. (f) EM-DCT$_{\mathrm{Dec.Thresh.}}$: 11.98 dB.

is complex and contains small and/or complex structures (see Fig. 4 versus Fig. 3).

The ability of our algorithm to filter out the residual noise in the reconstructed image (i.e., to decrease the variance within each structure of the resulting reconstructed images, see Figs. 2 and 3) is also clearly demonstrated. This is due to the result of the energy compaction of the DCT coding.

Finally, the decreasing sparsity strategy based on a cooling threshold schedule, frequently used in stochastic optimization [22], seems to be well suited to prevent the EM reconstruction procedure from becoming stuck in local minima. This gives a better chance of finding the best reconstruction, i.e., the one closest to the emission tomographic model (1) and with high sparsity property in the DCT domain.

To summarize, the above results from both synthetic and actual SPECT images clearly show that our approach performs very competitively as compared to, and is actually better than, the best existing methods. The decreasing sparsity constraint strategy seems particularly well suited to efficiently regularize the iterative EM tomographic reconstruction process. Moreover, we have shown that better results are obtained if the denoising step is made by a coefficient thresholding in the DCT[2] domain as compared to using a thresholding of undecimated discrete (redundant) wavelet coefficients [20] (similar conclusions have been arrived at with a soft thresholding operation).

[2]For the implementation of this step, we have used the very fast 8 × 8 (FFT2D) DCT package implemented in C code by Takuya Ooura (functions DDCT8X8S tested in program SHRTDCT.C) and available online at the address given in [23].

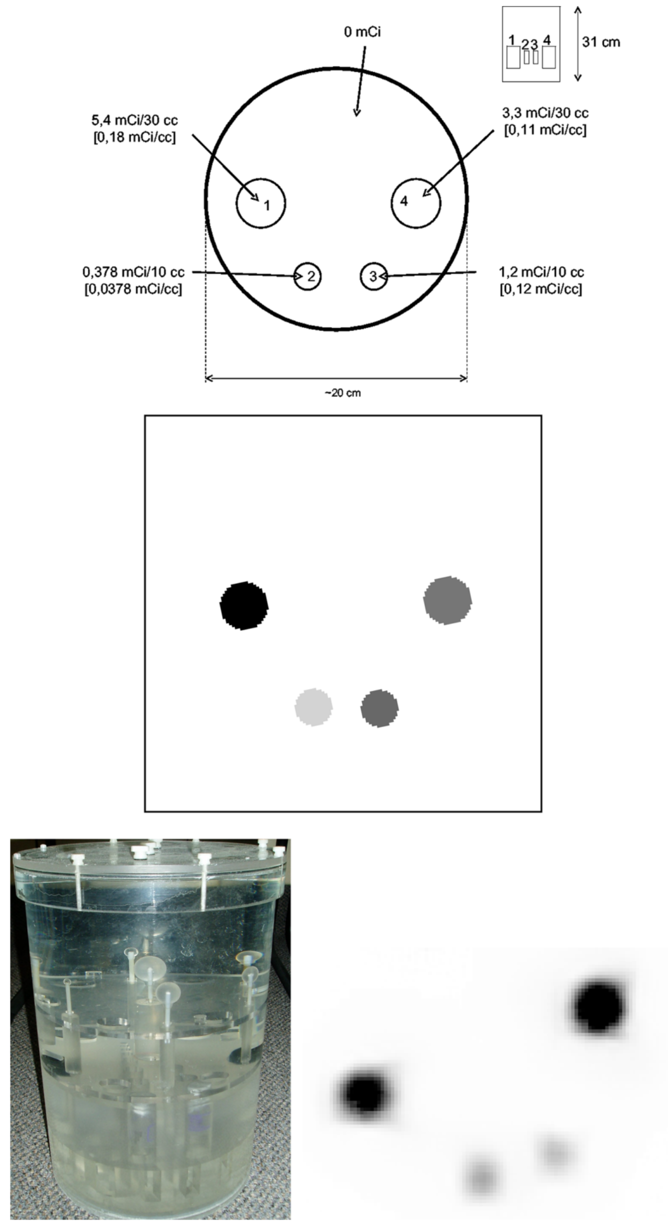

Fig. 4. Top: Cross-sectional view of the phantom showing the concentration of radioactivity within each of its subcompartments and cross-sectional "ground truth" (in inverse video) of the ideal SPECT reconstruction. Bottom left: Physical SPECT Phantom. Bottom right: EM-DCT$_{\mathrm{Dec.Thresh.}}$ reconstruction MSE $= \mathbf{313.42}$ (SNR $= \mathbf{7.70}$ dB) compared to GM: MSE $= \mathbf{330.80}$ (SNR $= \mathbf{7.47}$ dB), GGMRF$_{q=1.1}$: MSE $= \mathbf{339.63}$ (SNR $= \mathbf{7.35}$ dB), MEDIAN: MSE $= \mathbf{330.72}$ (SNR $= \mathbf{7.47}$ dB), EM-UDWT: MSE $= \mathbf{332.97}$ (SNR $= \mathbf{7.44}$ dB).

The computational time of the DCT regularization strategy using the above-mentioned fast DCT is negligible compared to the computational time of a ML-EM iteration. Notice that the denoising step can be easily implemented in parallel and that numerous fast very large scale integration (VLSI) chips exist for computing the DCT more rapidly.

VII. Conclusion

This paper has presented a simple algorithm based on a recursive sequence of ML-EM update and denoising operations combined with a decreasing threshold schedule in the DCT domain. The proposed method performs competitively when compared to recently reported Bayesian reconstruction strategies, while being simple and fast to implement. The same strategy with other basis functions (such as nonorthogonal redundant wavelets) seems to yield less good results in the specific context of SPECT tomographic reconstruction from projections.

ACKNOWLEDGMENT

The authors would like to thank the anonymous reviewers for helpful comments and suggestions which have contributed to improve this paper.

REFERENCES

[1] B. Mair, R. Carroll, and J. Anderson, "Filter banks and the em algorithm," in *Proc. Nucl. Sci. Symp., Conf. Record., IEEE Med. Imaging Conf.*, 1996, vol. 3, pp. 1747–1751.
[2] J. Kalifa, A. Laine, and P. D. Esser, "Regularization in tomographic reconstruction using thresholding estimators," *IEEE Trans. Med. Imag.*, vol. 22, no. 3, pp. 351–359, Mar. 2003.
[3] J.-W. Lin, A. F. Laine, and S. R. Bergmann, "Improving PET-based physiological quantification through methods of wavelet denoising," *IEEE Trans. Biomed. Eng.*, vol. 48, no. 2, pp. 202–212, Feb. 2001.
[4] M. Bhatia, W. Karl, and A. Willsky, "A wavelet-based method for multiscale tomographic reconstruction," *IEEE Trans. Med. Imag.*, vol. 15, no. 1, pp. 92–101, Feb. 1996.
[5] M. Bhatia, W. Karl, and A. Willsky, "Tomographic reconstruction and estimation based on multiscale natural-pixel bases," *IEEE Trans. Image Process.*, vol. 6, no. 3, pp. 463–478, Mar. 1997.
[6] B. Sahiner and A. Yagle, *Time Frequency and Wavelets in Biomedical Signal Processing*, M. Akay, Ed. Piscataway, NJ: IEEE Press, 1997, pp. 473–498.
[7] P. Green, "Bayesian reconstructions from emission tomography data using a modified EM algorithm," *IEEE Trans. Med. Imag.*, vol. 9, no. 1, pp. 84–93, Mar. 1990.
[8] H. Hudson and R. Larkin, "Accelerated image reconstruction using ordered subsets of projection data," *IEEE Trans. Med. Imag.*, vol. 13, no. 4, pp. 601–609, Dec. 1994.
[9] A. Dempster, N. Laird, and D. Rubin, "Maximum likelihood from incomplete data via the EM algorithm," *Royal Statistical Society*, pp. 1–38, 1976.
[10] L. A. Shepp and Y. vardi, "Maximum likelihood reconstruction for emission tomography," *IEEE Trans. Med. Imag.*, vol. 1, no. MI-2, pp. 113–122, Oct. 1982.
[11] B. Silverman, M. C. Jones, D. Nycha, and J. D. Wilson, "A smoothed em approach to indirect estimation problems, with particular reference to stereology and emission tomography," *J. R. Statist. Soc.*, ser. B, vol. 52, pp. 271–324, 1990.
[12] D. L. Donoho and I. M. Johnstone, "Ideal spatial adaptation by wavelet shrinkage," *Biometrika*, vol. 81, pp. 425–455, 1994.
[13] H. S. Malavar, *Signal Processing with Lapped Transforms*. Norwood, MA: Artech House, 1992.
[14] R. Coifman and D. Donohu, "Translation invariant denoising," in *Wavelets and Statistics*, A. Antoniadis and G. Oppenheim, Eds. New York: Springer-Verlag, 1995, vol. 103, Lecture Notes in Statistics, pp. 125–150.
[15] S. Furuie, G. Herman, T. Narayan, P. Kinahan, J. Karp, R. Lewitt, and S. Matej, "A methodology for testing for statistically significant differences between fully 3D PET reconstruction algorithms," *Phys. Med. Biol.*, no. 39, pp. 341–354, 1994.
[16] C. A. Bouman and K. Sauer, "A unified approach to statistical tomography using coordinate descent optimization," *IEEE Trans. Image Process.*, vol. 5, no. 3, pp. 480–492, Mar. 1996.
[17] K. Sauer and C. Bouman, "A local update strategy for iterative reconstruction from projections," *IEEE Trans. Signal Processing*, vol. 41, pp. 534–548, 1993.
[18] C. A. Bouman and K. Sauer, "A generalized Gaussian image model for edge-preserving MAP estimation," *IEEE Trans. Image Process.*, vol. 2, no. 3, pp. 296–310, Jul. 1993.
[19] I.-T. Hsiao and G. Gindi, "A new convex edge-preserving median prior with applications to tomography," *IEEE Trans. Med. Imag.*, vol. 22, no. 5, pp. 580–585, May 2003.
[20] G. Beylkin, "On the representation of operators in bases of compactly supported wavelets," *SIAM J. Numer. Anal.*, vol. 29, pp. 1716–1740, 1992.
[21] M. Lang, H. Guo, J. Odegard, C. B. amd, and R. O. Wells, "Noise reduction using an undecimated discrete wavelet transform," *IEEE Signal Process. Lett.*, vol. 3, no. 1, pp. 10–12, Jan. 1996.
[22] S. Geman and D. Geman, "Stochastic relaxation, Gibbs distributions and the Bayesian restoration of images," *IEEE Trans. Pattern Anal. Mach. Intell.*, vol. PAMI-6, no. 6, pp. 721–741, 1984.
[23] T. Ooura, "General purpose FFT (fast fourier/cosine/sine transform) package." [Online]. Available: http://momonga.t.u-tokyo.ac.jp/~ooura/fft.html

Extraction of Fetal Heart-Rate Signal as the Time Event Series From Evenly Sampled Data Acquired Using Doppler Ultrasound Technique

Janusz Jezewski*, Tomasz Kupka, and Krzysztof Horoba

***Abstract*—Analysis of variability of fetal heart rate (FHR) is very important in prediction of the fetal wellbeing. The beat-to-beat variability is described quantitatively by the indices originated from invasive fetal electrocardiography which provides the FHR signal in a form of time event series. Today, monitoring instrumentation is based on Doppler ultrasound technology. We used two bedside fetal monitors with different processing methods for heartbeat detection and FHR signal determination: the autocorrelation and cross-correlation techniques. Both monitors provide the output signal in a form of evenly spaced samples. The goal of this paper is to present a new method for the FHR signal processing, which enables extraction of series of consecutive heartbeat intervals from the sampled signal. The proposed correction algorithms allow recognition and removal of the FHR signal distortions typical for fetal monitors—invalid and duplicated samples. The correction efficiency has been verified based on the FHR variability indices calculated for the sampled signal and the corresponding event series. For both monitors, considerable influence of the signal representation on indices values was noted. Concluding, we recommended implementing these algorithms in fetal surveillance system as a preprocessing stage for the determination of FHR variability indices.**

***Index Terms*—Doppler ultrasound, fetal heart-rate (FHR) variability, heartbeat events.**

I. INTRODUCTION

Cardiotocography is an essential part of the present day perinatal medicine that allows monitoring of the fetus and evaluation of its state during pregnancy and labor. This method relies on recording of the fetal heart-rate signal (FHR) in relation to the uterine contractions and fetal movement activity. Based on a time interval T_i between two consecutive heartbeats, the instantaneous FHR_i value is calculated and is expressed in beats per minute (bpm). At the beginning of the 1970s,

Manuscript received December 14, 2006; revised May 20, 2007. This work was supported in part by the Ministry of Sciences and Higher Education resources in 2007–2009 under Research Project R13 028 02. *Asterisk indicates corresponding author.*

*J. Jezewski is with the Department of Biomedical Informatics, Institute of Medical Technology and Equipment, 118 Roosevelt St., Zabrze 41800, Poland (e-mail: jezewski@itam.zabrze.pl).

T. Kupka and K. Horoba are with the Department of Biomedical Informatics, Institute of Medical Technology and Equipment, Zabrze 41800, Poland (e-mail: tomekk@itam.zabrze.pl; kris@itam.zabrze.pl).

Digital Object Identifier 10.1109/TBME.2007.903532